Computerized Detection of Unruptured Aneurysms in MRA Images: Reduction of False Positives Using Anatomical Location Features

Yoshikazu Uchiyama[a], Xin Gao[a],Takeshi Hara[a], Hiroshi Fujita[a], Hiromichi Ando[b], Hiroyasu Yamakawa[c], Takahiko Asano[d], Hiroki Kato[d], Toru Iwama[e], Masayuki Kanematsu[d], Hiroaki Hoshi[d]

[a]Dept. of Intelligent Image Information, Graduate School of Medicine, Gifu Univ., Japan
[b]Dept. of Neurosurgery, Gifu Municipal Hospital, Japan
[c]Dept. of Neurosurgery, Matsunami General Hospital, Japan
[d]Dept. of Radiology, Graduate School of Medicine, Gifu University, Japan
[e]Dept. of Neurosurgery, Graduate School of Medicine, Gifu University, Japan

ABSTRACT

The detection of unruptured aneurysms is a major subject in magnetic resonance angiography (MRA). However, their accurate detection is often difficult because of the overlapping between the aneurysm and the adjacent vessels on maximum intensity projection images. The purpose of this study is to develop a computerized method for the detection of unruptured aneurysms in order to assist radiologists in image interpretation. The vessel regions were first segmented using gray-level thresholding and a region growing technique. The gradient concentration (GC) filter was then employed for the enhancement of the aneurysms. The initial candidates were identified in the GC image using a gray-level threshold. For the elimination of false positives (FPs), we determined shape features and an anatomical location feature. Finally, rule-based schemes and quadratic discriminant analysis were employed along with these features for distinguishing between the aneurysms and the FPs. The sensitivity for the detection of unruptured aneurysms was 90.0% with 1.52 FPs per patient. Our computerized scheme can be useful in assisting the radiologists in the detection of unruptured aneurysms in MRA images.

Keywords: Magnetic resonance angiography (MRA), Unruptured aneurysm, Gradient concentration filter, Anatomical location.

1. INTRODUCTION

Cerebrovascular diseases are the third leading cause of death in Japan.[1] Therefore, a screening system for the early detection of cerebral and cerebrovascular diseases, named *Brain Check-up*, is widely used in Japan. Because of the recent progress of magnetic resonance imaging (MRI), various types of cerebral diseases such as lacunar infarct, unruptured aneurysm, occlusion, and stenosis were detected in this screening system. Therefore, we developed computer-aided diagnosis (CAD) schemes for the detection of lacunar infarcts, unruptured aneurysms, and occlusions[2–6] in order to assist radiologists in image interpretation by the radiologists who use the computer outputs as a guide.

The detection of unruptured aneurysms in magnetic resonance angiography (MRA) studies is an important task because aneurysm rupture is the main cause of subarachnoid hemorrhage. However, it is often difficult for the radiologists to detect small aneurysms in the MRA studies because of the overlap between an aneurysm and the adjacent vessels on maximum intensity projection (MIP) images. Therefore, several CAD schemes for the detection of unruptured aneurysms in MRA studies have been reported.[4,7–10] In these schemes, shape features were generally used for distinguishing between the aneurysms and the normal vessels. It should be noted that unruptured aneurysms were often detected in the anterior communicating artery, branch points of middle cerebral artery, and branch points between the internal carotid artery and the posterior communicating artery. Therefore,

Corresponding author information: E-mail uchiyama@fjt.info.gifu-u.ac.jp.

Medical Imaging 2008: Computer-Aided Diagnosis, edited by Maryellen L. Giger, Nico Karssemeijer
Proc. of SPIE Vol. 6915, 69151Q, (2008) · 1605-7422/08/$18 · doi: 10.1117/12.770008

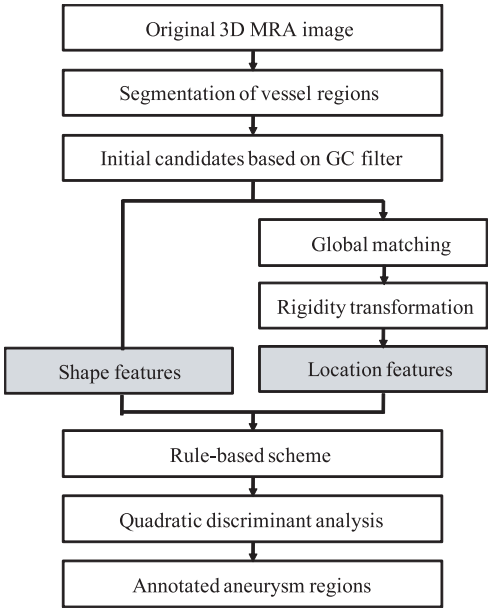

Figure 1. Overall scheme for the detection of unruptured aneurysms in 3D MRA images.

the anatomical location is an important information for the detection of unruptured aneurysms. However, there have been no reports on this method for the detection of unruptured aneurysms on the basis of anatomical location information.

In this study, we propose a method using the anatomical location feature for the detection of unruptured aneurysms. To obtain the anatomical location information, we employ an image registration technique along with a reference image so that the differences due to variations in the positioning of a patient can be adjusted. The adjusted locations in a common coordinate are used as the anatomical location feature. We will investigate the detection performance of our CAD schemes with and without anatomical location features and demonstrate the usefulness of anatomical location features for the detection of unruptured aneurysms in MRA images.

2. MATERIAL

A database consists of 100 MRA studies, including 72 normal and 28 abnormal with 30 unruptured aneurysms (diameter: 2.3 to 3.5 mm; mean: 2.8 mm). Eighteen of these MRA studies were performed using a 1.5 T magnetic image scanner (a Signa Excite Twin Speed 1.5 T; GE Medical Systems) at the Gifu University Hospital (Gifu, Japan). Each of these MRA studies includes 50 to 140 slice images. The axial slice images have a fixed size of 256×256 pixels, and the size of the pixels ranges from 0.625 mm to 0.78 mm. The thickness of each slice is in the range of 0.5 mm to 1.2 mm. The remaining 82 MRA studies were performed using a 1.5 T magnetic image scanner (Symphony; SIEMENS) at Gero Hot Springs Hospital (Gero, Japan). Each MRA study involves 72 to 80 slice images. The axial slice images have a size of either 256×192 or 256×176 pixels. Despite a slight variation in the image size, the axial slice images in all the 82 cases have the same pixel size and slice thickness of 0.7 mm and 1 mm, respectively. All the 100 studies were conducted by using a 3D time-of-flight technique. The acquired MRA data were subsequently converted to isotropic volume data by using linear interpolation. The size of the converted 3D volume data is $400 \times 400 \times 200$ voxels, and the size of each voxel is $0.5 \times 0.5 \times 0.5$ mm^3. The obtained isotropic volume data were employed in this study.

3. METHOD

3.1 Segmentation of Vessel Region

Figure 1 shows the overall scheme for the detection of unruptured aneurysms in MRA images. In order to avoid the false positives (FPs) located outside the vessel region, we first segmented the vessel regions. A linear

gray-level transformation was applied to the 3D MRA image so that the minimum voxel value became zero, and voxels with values greater than the 99% margin depicted in a cumulative histogram were assigned a maximum value of 1024. After the linear gray-level transformation, the vessel regions were segmented from the background by using the gray-level thresholding method with a threshold level of 700, which was selected empirically. Using this method, large vessels regions were successfully segmented. However, it was difficult to segment small vessels using this method because the voxel values in the small vessel regions were low. Therefore, a region growing technique was subsequently applied to segment the small vessel regions. The segmented large vessel regions were used as "seed" points, and the neighboring voxels with values greater than 500 were appended to the seed points.

3.2 Determination of Initial Aneurysm Candidates

For the enhancement of aneurysms, we applied a 3D gradient concentration (GC) filter[11,12] for the segmented vessel regions. This filter was designed to enhance the regions of a sphere by measuring the degree of convergence of the gradient vectors around a point of interest, which is defined by

$$GC(p) = \frac{1}{M} \sum_{R} \cos\theta_j \tag{1}$$

The output value of the GC filter at the point of interest $p(x, y, z)$ was computed within the regions of a sphere with a radius R at the center of $p(x, y, z)$. R was 5 voxels in this study. M is the number of voxels when the gradient magnitude located at $j(x, y, z)$ was greater than zero. The angle θ_j is the angle between the direction vector from $p(x, y, z)$ to $j(x, y, z)$ and the gradient direction vector located at $j(x, y, z)$. The gradient magnitude and gradient direction were determined by the first-order difference filter with a matrix size of $3 \times 3 \times 3$. For the identification of the initial aneurysm candidates, the gray-level thresholding technique with a threshold level of 0.5 was applied to the image obtained using the GC filter. After thresholding, we determined the initial candidates as the regions with a size larger than 10 voxels.

3.3 Features for Eliminating FPs

Using the techniques described in the previous section, almost all the aneurysms were detected accurately. However, the initially selected candidates also include many FPs. For eliminating these FPs, we used shape features and anatomical location features for distinguishing between the aneurysms and the FPs.

3.3.1 Shape Features

We used four features as the shape features, i.e., the size, degree of sphericity, and mean and maximum values of the GC image. The size was given as the number of voxels in the regions of the initial aneurysm candidate. The size may be useful a feature for eliminating the FPs because the sizes of some FPs were smaller or larger than those of the aneurysms. The degree of sphericity, which is defined by the fraction of the overlap volume of the candidate with a sphere having the same volume as the candidate, may also be a useful feature for distinguishing between the vessels and the aneurysms because some FPs were line-like or more irregular in comparison to the aneurysms. However, the degree of sphericity used in this study cannot find small dot-like objects such as aneurysms because it is difficult to quantify the shape of the surface accurately when the size of candidate is small. Thus, we used the mean and maximum values of the GC image in the candidate regions.

3.3.2 Anatomical Location Features

In order to obtain the anatomical location features, a reference (normal) MRA image was obtained by using the above-mentioned MR scanner at Gifu University Hospital. The acquired MRA images were subsequently converted to isotropic volume data by using linear interpolation. The vessel regions in the reference image were then semi-manually segmented for the image registration.

The segmented vessel regions in the target image were shifted to align with the reference image by using a global matching procedure and rigidity transformation. After the rigidity transformation, the locations x, y, and z in the target image were shifted into the common coordinate onto the reference image, thereby providing the anatomical location information.

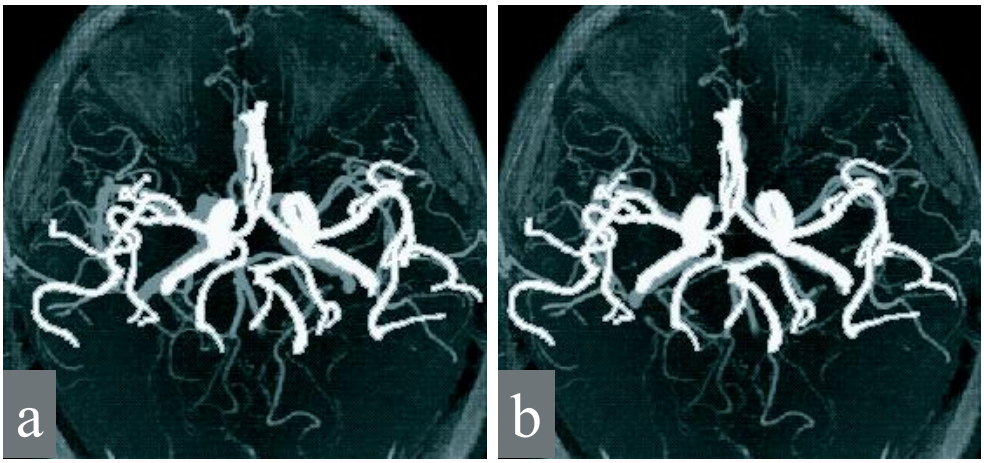

Figure 2. Illustration of global matching. The segmented vessel regions in a target 3D MRA image (white color) are superimposed onto the MIP image of the reference 3D MRA image (gray color): (a) Before global matching and (b) after global matching.

Global Matching

As the locations of the corresponding vessel regions in the target MRA image and the reference image are likely to be different due to the variations in the positioning of the patient, the registration of the corresponding vessel regions is necessary. Global matching was used for the initial image registration. In the global matching procedure, the translation vector was defined so as to maximize the overlapping of the vessel regions in the target image and reference image. Figure 2 shows the efficacy of global matching. By using this technique, the corresponding vessel regions in the two images were brought close to each other.

Corresponding Control Points

After the global matching procedure, rigidity transformation[13] was used to achieve a more accurate matching between the target image and the reference image. Twelve control points were pre-determined in the reference image, and the template matching method was used to determine the locations of the corresponding control points in the target image. In the template matching procedure, the normalized cross-correlation value C was used as a similarity measure. The cross-correlation between the template $A(i,j,k)$ containing a pre-determined feature point on the reference image and a region $B(i,j,k)$ containing a candidate corresponding to a feature point on the target image is given by

$$C = \frac{1}{IJK}\sum_{k=1}^{K}\sum_{j=1}^{J}\sum_{i=1}^{I}\frac{\{A(i,j,k)-\bar{a}\}\{B(i,j,k)-\bar{b}\}}{\sigma_A\sigma_B}, \tag{2}$$

$$\bar{a} = \frac{1}{IJK}\sum_{k=1}^{K}\sum_{j=1}^{J}\sum_{i=1}^{I}A(i,j,k), \bar{b} = \frac{1}{IJK}\sum_{k=1}^{K}\sum_{j=1}^{J}\sum_{i=1}^{I}B(i,j,k), \tag{3}$$

$$\sigma_A = \sqrt{\frac{\sum_{k=1}^{K}\sum_{j=1}^{J}\sum_{i=1}^{I}(A(i,j,k)-\bar{a})^2}{IJK}}, \tag{4}$$

$$\sigma_B = \sqrt{\frac{\sum_{k=1}^{K}\sum_{j=1}^{J}\sum_{i=1}^{I}(B(i,j,k)-\bar{b})^2}{IJK}}. \tag{5}$$

Here, $\bar{a}$ and σ_A are the average voxel value and standard deviation of template, respectively. The size of the template $I \times J \times K$ was set to be $21 \times 21 \times 21$. The normalized cross-correlation value indicates the resemblance between the reference and the template. If the images $A(i,j,k)$ and $B(i,j,k)$ are identical, C takes the value

1.0. Twelve templates were manually located in the cerebral region of the reference image. Figure 3 (a) shows the center points of the twelve templates in black dots. The search region associated with each template in the target image had a size of $41 \times 41 \times 41$. A set of coordinates of the corresponding points between the reference and the target images was determined by finding the largest cross-correlation value. Figure 3 (b) shows the 12 corresponding points found in the target image using the template matching method.

Rigidity Transformation

By using a set of corresponding control points determined by the template matching method, the translation and rotation vectors (T and R, respectively) were determined for the two images for rigidity transformation. Let P and p represent the corresponding points in the reference and the target images, respectively. Assuming that coordinates of the corresponding points in the images after global matching are $\{p_i = (x_i, y_i, z_i), P_i = (X_i, Y_i, Z_i) : i = 1, \cdots, 12\}$, the relation between the corresponding points in the images can be written as

$$P_i = Rp_i + T. \tag{6}$$

T and R can be determined by minimizing

$$E^2 = \sum_{i=1}^{P} \|P_i - (Rp_i + T)\|^2 . \tag{7}$$

An efficient algorithm was proposed for determining T and R in the reference.[14] In this algorithm, the rotation matrix is obtained first by minimizing

$$E_R^2 = \sum_{i=1}^{P} \|Q_i - R_i q_i\|^2 , \tag{8}$$

where $Q_i = P_i - \bar{P}$, $q_i = p_i - \bar{p}$, and $\bar{P}$ and $\bar{p}$ are the centers of gravity of the control points in the reference and target images, respectively. Further, considering the rotation matrix, T is determined using

$$T = P - Rp. \tag{9}$$

After rigidity transformation, the locations x, y, and z in the deformed target MRA image were shifted into the common coordinates on the reference image. The location on the reference image provides the anatomical location information.

3.3.3 Elimination of FPs

By applying the methods described in the previous sections to all the MRA images in our database, four shape features and three anatomical location features were obtained. The rules in our rule-based schemes were then set by using these values. First, we calculated the maximum and minimum values of each of these features obtained from all the aneurysms. All the 14 cutoff thresholds were determined on the basis of these values. The rule-based schemes were then used for the first step in the elimination of FPs, i.e., when a candidate was located outside the range determined by the cutoff thresholds in the feature space, the candidate was considered as an FP.

For further eliminating the FPs, we employed a quadratic discriminant analysis (QDA)[15] using four shape features and three location features. The QDA generates a decision boundary that optimally partitions the feature space into two classes, i.e., an aneurysm class and FP class. The decision boundary for the QDA was a quadratic surface given by a discriminant function. The output value of the discriminant function indicates the likelihood of the occurrence of the aneurysm. Thus, we can classify the aneurysm candidates into true positive class and FP class by partitioning the feature space using the threshold level of the discriminant function. By changing the threshold level, we can determine the performance for the detection of aneurysms using our computerized scheme.

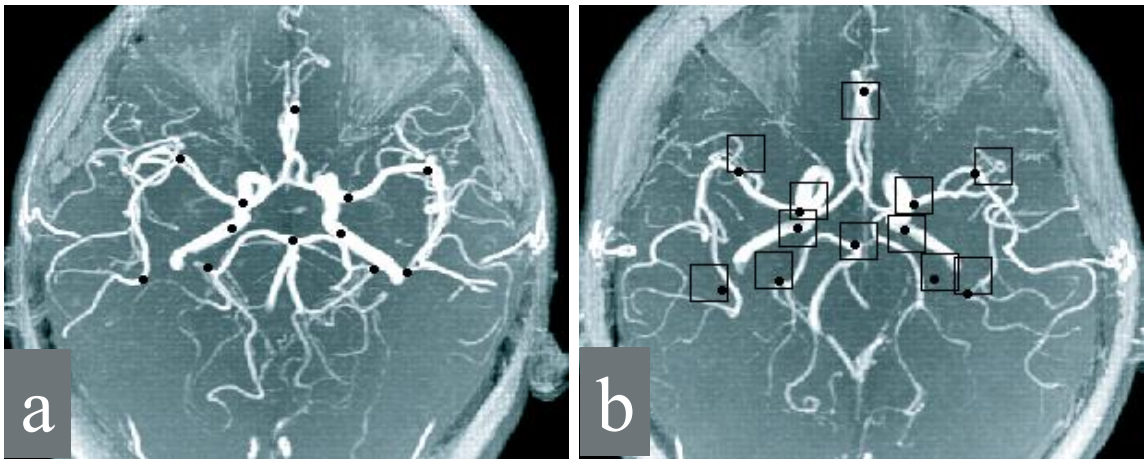

Figure 3. Corresponding control points for rigidity transformation. (a) The center points of the 12 templates (black dots) projected onto the MIP image of the reference MRA study. (b) Corresponding point (black dots) in the MIP image of the target MRA study were located using the template matching method. Square boxes indicate the search areas for individual control points.

4. RESULTS

Our method was applied to 100 clinical cases. As the first step toward identifying the initial candidates for aneurysms, 93.3% (28/30) aneurysms were accurately detected with 27.32 (2732/100) FPs per patient. This result indicated that the GC filter was useful in the detection of aneurysms because almost all the aneurysms were detected accurately. However, many FPs were also detected using this method.

For the elimination of the FPs, we determined four shape features and three location features. By using rule-based schemes with these features, our CAD scheme obtained a sensitivity of 90.0% (27/30) with 7.00 (700/100) FPs per patient. Thus, 74.4% of the FPs were eliminated using this scheme. This result indicates that the features determined in this study were useful for distinguishing between the aneurysms and the FPs.

For the further elimination of the FPs, a QDA with the same features was employed for distinguishing between the aneurysms and the FPs. The results revealed that our CAD scheme achieved that the same sensitivity of 90.0% (27/30) with 1.52 (152/100) FPs per patient. In order to investigate the usefulness of location features, we also calculated the detection performance of our CAD scheme without the location features. Figure 4 shows the free-response receiver operating characteristic (FROC) curves[16] for the overall performance of the detection of aneurysms with and without location features. The graphs show that the number of FPs decreased from 3.47 (without location features) to 1.52 (with location features) while maintaining a sensitivity of 90.0%. Thus, we believe that location features was useful for distinguishing between the aneurysms and the FPs.

5. CONCLUSIONS

We developed a computerized method for the detection of unruptured aneurysms in MRA images by using location features. The sensitivity of the detection of aneurysms was 90.0% with 1.52 FPs per patients. Therefore, our computerized scheme could be useful in assisting the radiologists in correctly identifying the aneurysms and for reducing the time required for interpretation.

ACKNOWLEDGMENTS

This work was partly supported by a grant for the Knowledge Cluster Creation Project from the Ministry of Education, Culture, Sports, Science and Technology, Japan.

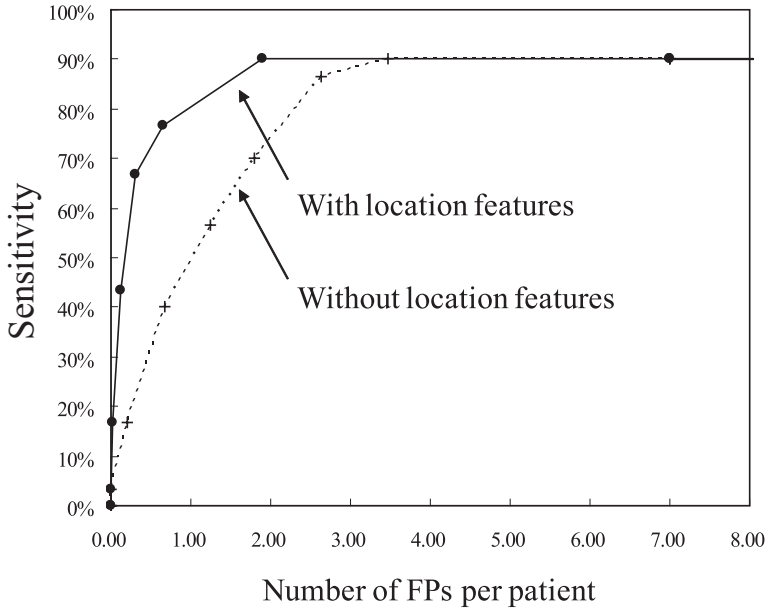

Figure 4. FROC curves for the overall performance of our computerized scheme in the detection of aneurysms in MRA images with and without location features.

REFERENCES

1. Health and W. S. Association, *Vital Statistics of Japan*, Daiwa Sougou Insatu, Tokyo, 2003.
2. R. Yokoyama, X. Zhang, Y. Uchiyama, H. Fujita, T. Hara, X. Zhou, M. Kanematsu, T. Asano, H. Kondo, S. Goshima, H. Hoshi, and T. Iwama, "Development of an automated method for detection of chronic lacunar infarct regions on brain MR images," *IEICE Trans. Inf. Syst.* **E90-D(6)**, pp. 943–954, 2007.
3. Y. Uchiyama, R. Yokoyama, H. Ando, T. Asano, H. Kato, H. Yamakawa, H. Yamakawa, T. Hara, T. Iwama, H. Hoshi, and H. Fujita, "Computer-aided diagnosis scheme for detection of lacunar infarcts on MR image," *Academic Radiology* **14(12)**, pp. 1554–1561, 2007.
4. Y. Uchiyama, H. Ando, R. Yokoyama, T. Hara, H. Fujita, and T. Iwama, "Computer-aided diagnosis scheme for detection of unruptured intracranial aneurysms in MR angiography," *Proc of IEEE Engineering in Medicine and Biology 27th Annual International Conference* **1**, pp. 3031–3034, 2005.
5. Y. Uchiyama, M. Yamauchi, H. Ando, R. Yokoyama, T. Hara, H. Fujita, T. Iwama, and H. Hoshi, "Automated classification of cerebral arteries in MRA images and its application to maximum intensity projection," *Proc of IEEE Engineering in Medicine and Biology 28th Annual International Conference* **1**, pp. 4865–4868, 2006.
6. M. Yamauchi, Y. Uchiyama, R. Yokoyama, T. Hara, H. Fujita, H. Ando, H. Yamakawa, T. Iwama, and H. Hoshi, "Computerized scheme for detection of arterial occlusion in brain MRA images," *Proc. of SPIE Medical Imaging : Computer-Aided Diagnosis* **6514**, pp. 65142C–1–65142C–9, 2007.
7. H. Arimura, Q. Li, Y. Korogi, T. Hirai, H. Abe, Y. Yamashita, S. Katsuragawa, R. Ikeda, and K. Doi, "Automated computerized scheme for detection of unruptured intracranial aneurysms in three-dimensional MRA," *Academic Radiology* **11**, pp. 1093–1104, 2004.
8. H. Arimura, Q. Li, Y. Korogi, T. Hirai, S. Katsuragawa, Y. Yamashita, K. Tsuchiya, and K. Doi, "Computerized detection of intracranial aneurysms for three-dimensional mr angiography: Feature extraction of small protrusions based on a shape-based difference image technique," *Medical Physics* **33**, pp. 394–401, 2006.

9. H. Hayashi, Y. Masutani, T. Matsumoto, H. Mori, A. Kunimatsu, O. Abe, S. Aoki, K. Ohtomo, N. Takano, and K. Matsumoto, "Feasibility of a curvature-based enhanced display system for detecting cerebral aneurysms in MR angiography," *Magnetic Resonance in Medical Science* **2**, pp. 29–36, 2003.
10. S. Kobayashi, K. Kondo, and Y. Hata, "Computer-aided diagnosis of intracranial aneurysms in MRA images with case-based reasoning," *IEICE Trans. Info. Syst.* **E89-D(1)**, pp. 340–350, 2006.
11. K. Kobatake and S. Hashimoto, "Convergence index filter for vector fields," *IEEE Trans on Image Processing* **8(8)**, pp. 1029–1038, 1999.
12. J. Nappi and H. Yoshida, "Automated detection of polyps with CT colonography: Evaluation of volumetric features for reduction of false-positive finding," *Academic Radiology* **9(4)**, pp. 386–397, 2002.
13. A. A. Goshtasby, *2-D and 3-D image registration*, John Wiley Sons, Inc. Hoboken, New Jersey, 2005.
14. K. S. Arum, T. S. Huang, and S. D. Blostein, "Least-square filtering of two 3-D point sets," *IEEE Trans. on Pattern Analysis and Machine Intelligence* **9(5)**, pp. 698–700, 1987.
15. K. Fukunaga, *Introduction to statistical pattern recognition*, Academic Press, San Diego, 1990.
16. D. P. Chakraborty, "Maximum likelihood analysis of free-response receiver operating characteristic (FROC) data," *Medical Physics* **16(4)**, pp. 561–568, 1989.